Supporting Information

for

Closed-Loop Nanopatterning of Liquids with Dip-Pen Nanolithography

Verda Saygin,[†] Bowen Xu,[†] Sean B. Andersson,[†‡] Keith A. Brown[*†§]

[†]Department of Mechanical Engineering, Boston University, 110 Cummington Mall, Boston, Massachusetts 02215, United States.

[‡]Division of Systems Engineering, Boston University, 110 Cummington Mall, Boston, Massachusetts 02215, United States.

[§]Physics Department and Division of Materials Science and Engineering, Boston University, 590 Commonwealth Avenue, Boston, Massachusetts 02215, United States.

***Corresponding Author**
*Keith A. Brown
Department of Mechanical Engineering, Physics Department, and Division of Materials Science and Engineering, Boston University, Boston, Massachusetts 02215, United States
orcid.org/0000-0002-2379-2018
Email: brownka@bu.edu

1. Drop Dynamics on Conical Probes

Conventional dip-pen nanolithography (DPN) utilizes hydrophilic atomic force microscopy (AFM) probes with conical tips where the ink covers the tip and the cantilever beam completely as a film. However, quantifying the loaded ink on the cantilever from the resonance frequency shift requires a discrete pendant drop. Drops on cones can adopt two different morphologies, namely a "barrel" and a "clamshell".[1] The behavior of the drop depends on its volume, the sharpness of the cone, and the contact angle between the liquid and the surface. When the drop is large, it will adopt the barrel configuration (Figure S1-A,B). In this configuration, the local substrate curvatures are substantially different at two opposing sides of the drop, which results in a difference in the Laplace pressure that drives the drop towards to base of the cantilever.[2] Figure S1-B shows that the outcome of this process in which the loaded ink does not cover the tip of the cone, making this configuration unsuitable for patterning since the liquid cannot come into contact with the substrate for patterning when the probe is brought into contact with a surface. If, in contrast, the drop is small or the contact angle is too high, the drop adopts the clamshell configuration (Figure S1-C,D,E). The position of the drop in this case cannot be controlled, and it is not suitable for patterning since it does not cover the tip.

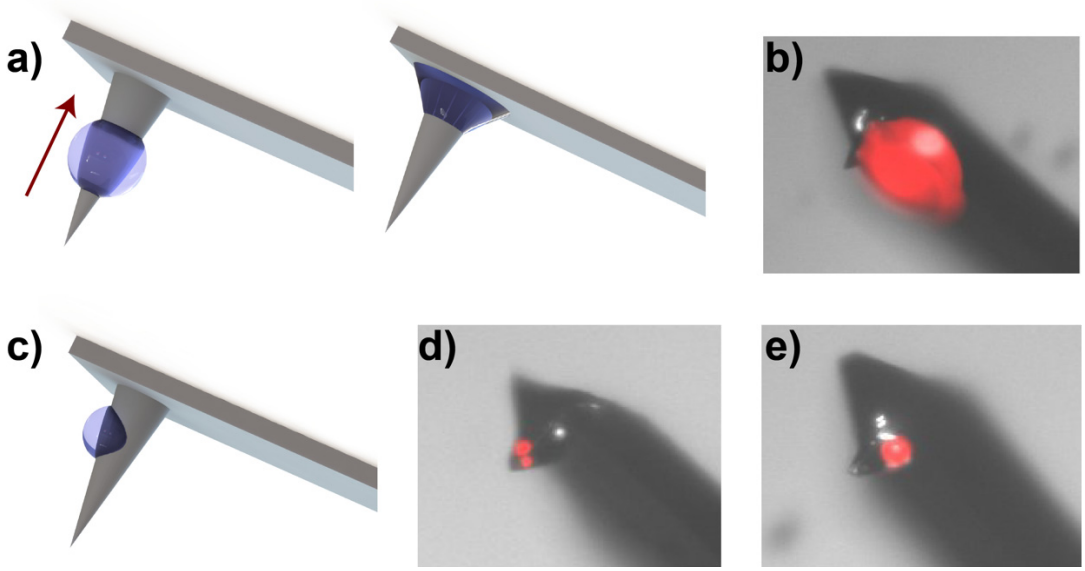

Figure S1. Two configurations a discrete drop can adopt on a conical tip. (a) In the "barrel" configuration, the drop engulfs the conical tip and is compelled to move towards the base of the conical probe. (b) Fluorescence micrograph of an inked probe showing a drop sitting on the base of the conical probe and not covering the probe tip. (c) If the contact angle is high or the drop volume is small, the drop sits on the probe in the "clamshell" configuration. (d,e) Fluorescence micrographs of an inked probe with small drops show on the side of the conical probe that do not cover the probe tip.

2. Calculation of Cantilever Mass

The first vibrational resonance frequency f_0 of a cantilever can be defined as,

$$f_0 = \frac{1}{2\pi}\sqrt{\frac{k}{m_{eff}}}, \quad (1)$$

where m_{eff} is the effective mass of the cantilever and k is its spring constant. The relationship between the effective mass of a cantilever and its actual mass M is given by $m_{eff} = \alpha M$, where the coefficient α is a dimensionless parameter that only depends on the cantilever shape and is independent of its absolute dimensions. For a rectangular cantilever with an aspect ratio (defined as cantilever length over width) less than 0.2, this coefficient is $\alpha = 0.2427$.[3,4] Thus, Equation (1) may be rewritten to find,

$$M = k/\alpha(2\pi f_0)^2. \quad (2)$$

As both k and f_0 can be robustly measured using the AFM system, Equation (2) allows one to estimate M.

3. Capillary Force During Patterning and Probe Selection

When the AFM probe with a pendant drop is brought into contact with a surface, a capillary bridge is formed between the probe and the substrate. This liquid bridge results in an attractive capillary force between the probe and substrate, the magnitude of which depends on the liquid surface tension, the wettability of both surfaces, and the volume of the liquid. Figure S2 shows force-distance and deflection-distance curves obtained during patterning of a polyisobutylene (PIB) feature. Here, the cantilever used in the experiment had k = 3.16 N/m, with liquid mass m_l = 2.33 ng. The maximum capillary force F applied observed was 2.3 μN, which led the cantilever to deflect as much as ~700 nm. The AFM system has a piezo range of 11 μm in the z direction, hence, this capillary bridge could be ruptured using our system. However, in the case of using a softer cantilever (*i.e.* one with k that is smaller in magnitude), deflection would be larger and could easily reach several micrometers, thus limiting our ability to break the capillary bridge while under piezoelectric control. As a result, the stiffness of the AFM probe should be chosen according to the piezo retraction limit and maximum allowable deflection caused by the capillary bridge.

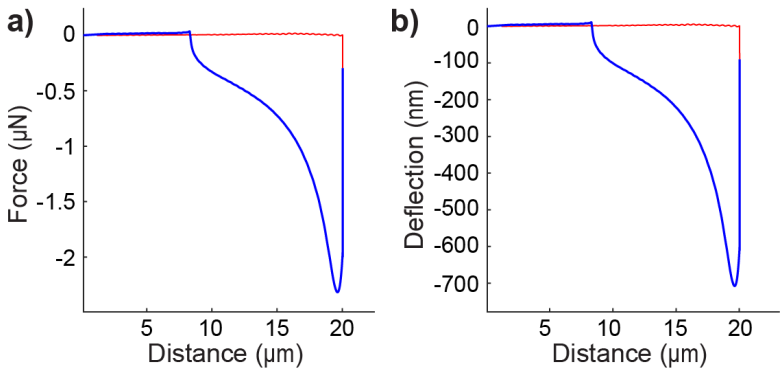

Figure S2. (a) Force-distance and (b) deflection-distance curves for a force-distance curve performed while writing a feature of PIB using a tipless probe.

4. Liquid Selection

Potential liquids for patterning were evaluated in three categories. Specifically, successful patterning requires reliable liquid-substrate contact and the formation of a pendant drop to facilitate inertial sensing of the liquid. To meet these criteria, the chosen liquid should have a high surface energy to prevent wetting. Further, precise inertial-sensing can only be achieved if the liquid mass is not being reduced through the evaporation of the liquid, which requires that the liquid is non-volatile. It is worth emphasizing that this criterion can be relaxed in circumstances when the transport mechanics are not the focus of the study. To evaluate potential liquids of interest, we construct a radar chart showing the qualitative properties of a number of candidate liquids (Figure S3). This analysis reveals that glycerol is not a suitable option due to its volatility even though it has high surface energy. In contrast, silicon oil is not suitable due to its low surface energy, even though it is non-volatile. Both PIB and poly(ethylene glycol) diacrylate (PEGDA) are non-volatile and have high surface energies, hence both were experimentally investigated as liquids of interest for our patterning experiments. Ultimately, studies of the transport mechanism revealed that high viscosity is ideal for affording control over the patterning process, leading to the selection of PIB as an ideal liquid for patterning.

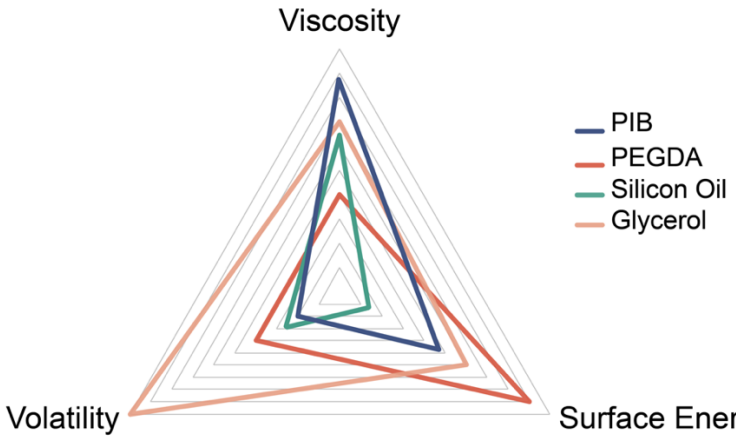

Figure S3. Qualitative radar chart showing the comparison of three characteristic properties for four liquids of interest, namely polyisobutylene (PIB), poly(ethylene glycol) diacrylate (PEGDA), silicon oil, and glycerol.

5. Variation of Transfer Properties

Liquid transfer between two surfaces depends on material properties, cantilever speed, the wettability of the surfaces, and to a lesser extent the ambient relative humidity and temperature. There are 4 major parameters that can be controlled during liquid transfer with AFM. Approach speed of the cantilever U_a, the force setpoint, dwell time t_d and retraction speed U. A force-time curve for a feature write is shown in Figure S4. We selected U_a, t_d to allow robust patterning and kept these parameters constant for all patterning experiments to ensure that the capillary bridge was static before rupture.

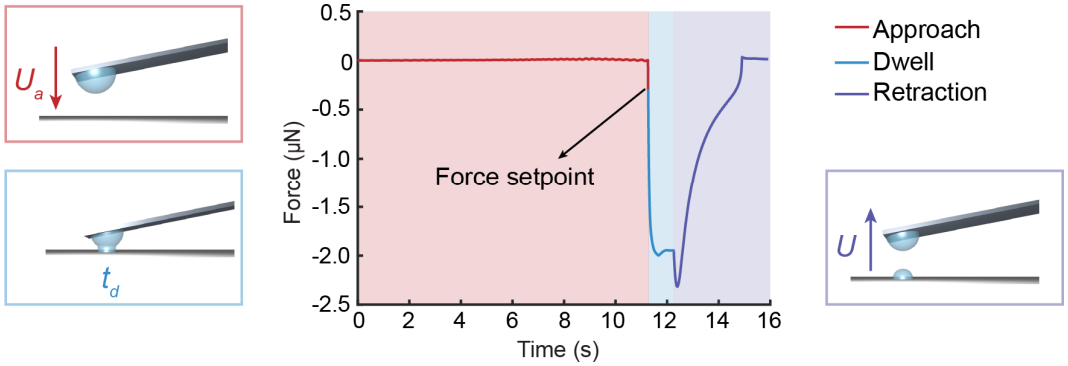

Figure S4. Force-time curve for a patterned feature and respective configurations of the cantilever during patterning with writing parameters that are controlled by the AFM.

Typical patterning experiments were conducted under ambient conditions, where slight changes in relative humidity or temperature can in principle affect liquid transfer even when the substrate, probe, and liquid are nominally the same. In order to explore this, calibration

experiments were repeated on multiple days to produce a series of transfer ratio φ vs. U curves (Figure S5). The data collected on each day was fit to,

$$\varphi = 0.5 + (\varphi_0 - 0.5/1 + (\frac{U}{U_c})^a), \quad (3)$$

where ϕ_0 is the asymptotic transfer ratio in the quasi-static regime, which is the lowest achievable transfer ratio, a is an empirical power law that describes transport, and U_c is a characteristic velocity. The results of this analysis for three experiments conducted on different days is given in Table S1. We hypothesize that the observed variation in fitting parameters is due to the effect of environmental conditions on liquid transfer. These results show that it is not possible to rely exclusively on data collected on prior days to calibrate patterning experiments.

Table S1: Fitting parameters for experimental φ vs. U data fit to Equation (3).

	φ_0	U_c [μm s^{-1}]	a
Experiment 1	0.186 ± 0.006	23.129 ± 2.046	1.705 ± 0.119
Experiment 2	0.125 ± 0.006	19.710 ± 2.125	1.573 ± 0.101
Experiment 3	0.119 ± 0.008	22.928 ± 3.086	1.501 ± 0.146

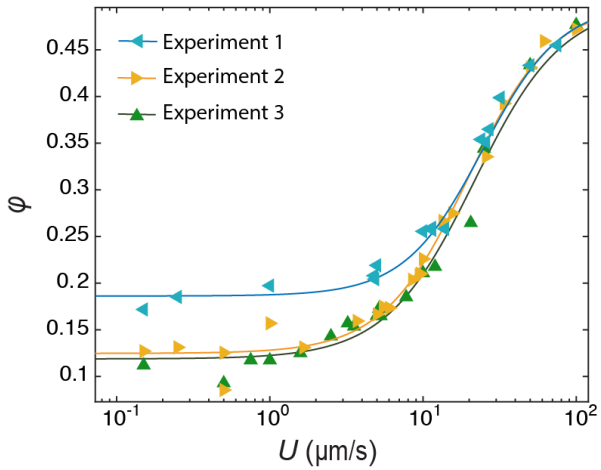

Figure S5. Experimental φ vs. U in the full range available to the AFM system for patterning experiments of PIB performed on different days with the same probe.

6. Details of the Molecule Pattern

In order to evaluate the ability of DPN with closed-loop feedback to generate patterns with generality, we performed an experiment attempting to pattern the molecular formula of the molecule ethanol (Figure S6). Features masses were chosen according to the atomic masses of carbon, oxygen, and hydrogen, which are C : O : H = 12 : 16 : 1.

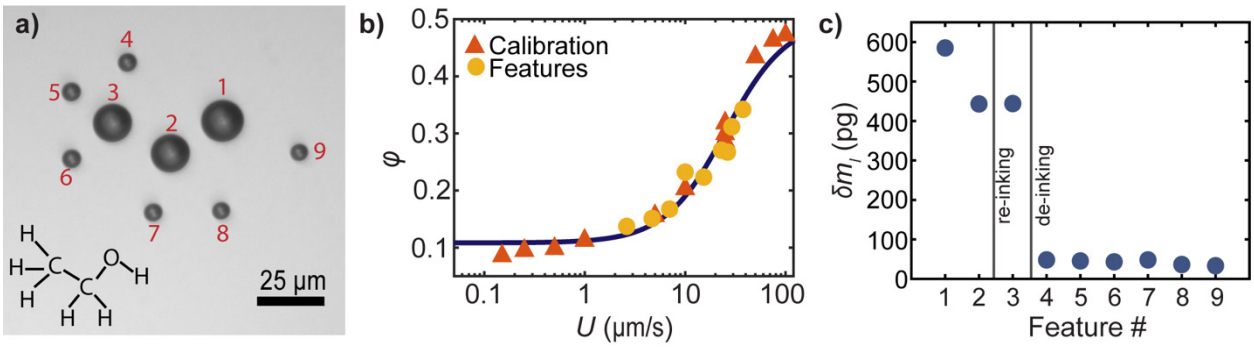

Figure S6. (a) Bright field optical micrograph of the result of a patterning demonstration showing a schematic depicting the chemical formula of ethanol. The inset shows the template formula including two carbon atoms, one oxygen atom, and six hydrogen atoms. (b) Experimental φ vs. U collected as part of the patterning experiment. This process included nine calibration features and nine features written as part of the pattern. (c) Inertially determined masses of the written features δm_l, where feature 1 corresponds to the oxygen atom, features 2 and 3 correspond to the carbon atoms, and features 4-9 correspond to the hydrogen atoms. The experiment includes a re-inking step between patterning the two carbon atoms to increase ink on the probe and one de-inking step before patterning the hydrogen atoms to decrease the ink on the probe.

7. Mass Resolution Study

The mass resolution possible when patterning with a tipless cantilever was studied by patterning features with a constant retraction speed of 0.25 μm/s. In order to span the gamut of available feature size, the probe was not reinked during the writing process. Figure S7a shows features patterned with a rectangular cantilever with $f_1 \approx 80$ kHz and $k = 3.1$ N/m. For this cantilever, which has the same properties as those used in the main text figures of this study, f_1 was small enough that the second harmonic mode was observable in a thermal measurement, hence the transferred masses of these features were determined using the cantilever bending model and showed on Figure S7b. In addition, the volume V_o of these features was estimated by measuring their diameters from the optical micrograph. The precision of the mass sensing scheme was estimated by fitting $\delta m_l = \alpha V_0$ and examining the mean absolute residual of the fit, which was found to be 2.4 pg.

To investigate whether more accurate writing would be possible with different probes, a 5 × 5 grid of PIB features was patterned using a stiff cantilever with $f_1 \approx 304$ kHz and $k = 26.8$ N/m (Figure S7c). While f_1 for this cantilever was too high to allow us to measure the second harmonic mode, meaning that δm_l was estimated using only the first mode, the comparatively high resonance frequency of the first harmonic mode enables a greater sensitivity for the mass detection. Specifically, while the soft cantilever's sensitivity was predicted to be 0.35 pg/Hz, the stiffer cantilever had a sensitivity of 0.049 pg/Hz. Since both the patterned features and drop on the cantilever were small, we performed the analysis under the assumption that the drop position

did not change from $x/L = 0.99$ over the course of patterning. Needing only a single mode, we measured the resonance frequency using active tuning rather than measurements of the thermal power spectral density (PSD). Repeating the process of estimating the precision of mass sensing as the mean absolute residual of the fit to $\delta m_l = \alpha V_0$ revealed the precision of this probe to be 20 fg (Figure S7d).

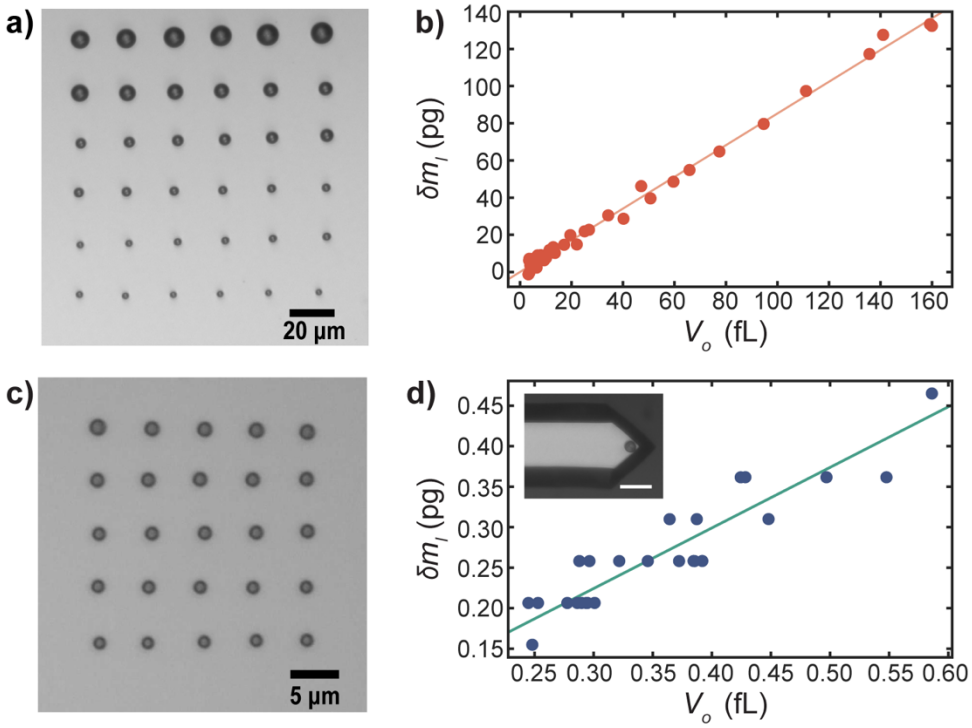

Figure S7. (a) Bright field optical micrograph of PIB features written with a constant retraction speed using a soft tipless cantilever. (b) Inertially determined δm_l of the patterned features in (a) computed using the cantilever bending model and the patterned feature volume V_o determined using optical microscopy. (c) Bright field optical micrograph of PIB features written with a constant retraction speed using a stiff tipless cantilever. (d) Inertially determined δm_l from (c) estimated using a single harmonic mode vs. V_o. The inset shows a bright field optical micrograph of the cantilever with a PIB drop and includes a 15 µm scale bar. The position of the PIB drop on the cantilever was estimated using the optical micrograph.

8. Supporting References

(1) McCarthy, J.; Vella, D.; Castrejón-Pita, A. A. Dynamics of Droplets on Cones: Self-Propulsion Due to Curvature Gradients. *Soft Matter* **2019**, *15* (48), 9997–10004. https://doi.org/10.1039/c9sm01635j.

(2) Li, Y.; Wu, H.; Wang, F. Stagnation of a Droplet on a Conical Substrate Determined by the Critical Curvature Ratio. *J. Phys. D. Appl. Phys.* **2016**, *49* (8), 85304. https://doi.org/10.1088/0022-3727/49/8/085304.
(3) Chen, G. Y.; Warmack, R. J.; Thundat, T.; Allison, D. P.; Huang, A. Resonance Response of Scanning Force Microscopy Cantilevers. *Rev. Sci. Instrum.* **1994**, *65* (8), 2532–2537. https://doi.org/10.1063/1.1144647.
(4) Sader, J. E.; Larson, I.; Mulvaney, P.; White, L. R. Method for the Calibration of Atomic Force Microscope Cantilevers. *Rev. Sci. Instrum.* **1995**, *66* (7), 3789–3798. https://doi.org/10.1063/1.1145439.